UC Santa Barbara

Title

A pattern-based definition of urban context using remote sensing and GIS

Permalink

https://escholarship.org/uc/item/4580m0n4

Authors

Benza, Magdalena
Weeks, John R
Stow, Douglas A
et al.

Publication Date

2016-09-01

DOI

10.1016/j.rse.2016.06.011

Peer reviewed

HHS Public Access

A Pattern-Based Definition of Urban Context Using Remote Sensing and GIS

Magdalena Benza[a], **John R. Weeks**[a], **Douglas A. Stow**[a], **David López-Carr**[b], and **Keith C. Clarke**[b]

[a]Department of Geography, San Diego State University, 5500 Campanile Dr., San Diego, CA 92182-4493, United States

[b]Department of Geography, 1832 Ellison Hall, University of California Santa Barbara, Santa Barbara, CA 93106-4060, United States

Abstract

In Sub-Saharan Africa rapid urban growth combined with rising poverty is creating diverse urban environments, the nature of which are not adequately captured by a simple urban-rural dichotomy. This paper proposes an alternative classification scheme for urban mapping based on a gradient approach for the southern portion of the West African country of Ghana. Landsat Enhanced Thematic Mapper Plus (ETM+) and European Remote Sensing Satellite-2 (ERS-2) synthetic aperture radar (SAR) imagery are used to generate a pattern based definition of the urban context. Spectral mixture analysis (SMA) is used to classify a Landsat scene into Built, Vegetation and Other land covers. Landscape metrics are estimated for Built and Vegetation land covers for a 450 meter uniform grid covering the study area. A measure of texture is extracted from the SAR imagery and classified as Built/Non-built. SMA based measures of Built and Vegetation fragmentation are combined with SAR texture based Built/Non-built maps through a decision tree classifier to generate a nine class urban context map capturing the transition from unsettled land at one end of the gradient to the compact urban core at the other end. Training and testing of the decision tree classifier was done using very high spatial resolution reference imagery from Google Earth. An overall classification agreement of 77% was determined for the nine-class urban context map, with user's accuracy (commission errors) being lower than producer's accuracy (omission errors). Nine urban contexts were classified and then compared with data from the 2000 Census of Ghana. Results suggest that the urban classes appropriately differentiate areas along the urban gradient.

Corresponding author: Magdalena Benza, Department of Geography, San Diego State University, 5500 Campanile Dr., San Diego, CA 92182-4493, United States, magdalena.benza@gmail.com, tel: +1-202-716-9845.

1. Introduction

In the coming decades most of the world's land cover and land use change (LCLUC) is predicted to take place in the tropics, where population is growing the fastest (DeFries, Asner and Foley 2006). United Nations' projections estimate that virtually all of the world's population between now and the middle of this century will emerge in the cities of the developing world, (United Nations Population Division 2012) driven by natural increase in both urban and rural areas, and by continued migration from rural to urban areas as people search for economic opportunities (Lee 2007). Urbanization is shaping landscapes in and around cities through densification and sprawl, while at the same time increased interaction among cities is creating new hybrid landscapes where rural and urban livelihoods overlap (Lambin et al. 2001, Seto et al. 2012). The rapid pace of recent urbanization is reshaping the morphology and function of cities around the world (Longley 2002), and while research has found that urban growth and the demand for land conversion has been driving habitat fragmentation (Wickham, O'Neill and Jones 2000), little is known about how the urban landscape itself is changing as cities grow (Liu and Herold 2007, Seto and Shepherd 2009). Urban environments are becoming increasingly diverse and a simple urban-rural dichotomy fails to capture that diversity (Champion and Hugo 2004).

Urban mapping increasingly relies on the use of satellite imagery through the development of objective, automated and replicable methodologies for the identification of human-induced land covers (Pumain 2004). The physical characteristics of urban places generate spatial and spectral signatures that are readily captured in remotely sensed data (Elvidge et al. 2004). As a result, detection and monitoring of the urban environment at global, regional and local scales depends more and more on the use of such data (Potere et al. 2009, Small 2005, Lu and Weng 2006). In developing countries, where urbanization is taking place at the fastest rates (United Nations Population Division 2014), the geographic comprehensiveness of satellite imagery has made it a useful tool for quantifying and monitoring the distribution and growth of human settlements (Harris and Longley 2002, Weeks 2004). The Landsat Thematic Mapper (TM), Enhanced Thematic Mapper Plus (ETM+) and Operational Land Imager (OLI) satellite systems provide an extensive and accessible archive of moderate spatial resolution (~30 m) imagery that has been successfully used to monitor urban areas and settlements in a wide range of environments (Small 2005, Seto and Fragkias 2005, Lu and Weng 2008). In equatorial and tropical regions where cloud cover is a common problem for optical remote sensing, radar imagery is an alternative data source (Rogan et al. 2003) that has successfully been used for human settlement detection (Stasolla and Gamba 2008) and for urban mapping (Haack and Bechdol 2000). While measures of texture extracted from the Synthetic Aperture Radar (SAR) imagery have been found to improve land cover and land use mapping (Herold, Haack and Solomon 2004), detect building density (Dell'Acqua and Gamba 2003) and differentiate informal from formal settlements (Dell'Acqua, Stasolla and Gamba 2006), applications that combine radar and optical imagery have shown to successfully detect human settlements (Haack et al. 2002, Tatem, Noor and Hay 2004).

Definitions of settlements as urban are generally based on an arbitrary threshold set as the split between rural and urban places without accounting for differences in land use intensity,

function or heterogeneity (Seto et al. 2012). However, in urban environments different types and densities of buildings and built surface materials, as well as vegetation, can vary within short distances (Cadenasso, Pickett and Schwarz 2007). Rising suburbanization trends are forming edge cities that are increasingly facilitating urban spread into rural areas (Zipperer et al. 2000) and blurring the distinctions between rural and urban places (Hugo, Champion and Lattes 2003). The diffuse transition between urban centers and the countryside is described by Antrop (2004) as a complex combination of land uses with diverse and fragmented morphology. This heterogeneous transition zone that extends between urban and rural places requires further identification and classification.

Although most research on urban spaces continues to use a simple urban-rural dichotomy, there have been attempts to characterize urban environments through gradient approaches based on measures of landscape fragmentation. Research on urban ecosystems has focused on examining the interaction between habitat fragmentation and ecological function (Breuste, Niemelä and Snep 2008, Kühn and Klotz 2006). Measures of landscape fragmentation have also been used in studies of spatial patterns of urban form (Yang et al. 2011, Van de Voorde, Jacquet and Canters 2011) and growth (Luck and Wu 2002, Weng 2007). Research in the fields of landscape ecology and population have proposed the use of continuous measures of degree of urbanization that combine proportions of land cover with population characteristics (McDonnell and Hahs 2008, Weeks, Larson and Rashed 2003), and measures of landscape pattern with socio-economic indicators (Toit and Cilliers 2011, Weeks, Larson and Fugate 2005). These studies that integrate data collected in censuses or surveys with imagery derived data have two disadvantages: (a) an urban gradient cannot be calculated in the absence of those socioeconomic data; and (b) since its definition depends upon such data, an urban gradient cannot –without becoming tautological-be used directly to predict a population's socioeconomic characteristics. The objective of this study is to develop and test a pattern-based classification scheme for the urban context, using an gradient approach based solely on remotely sensed imagery that exploits quantitative measures of spatial patterns of built and vegetation land cover for the purpose of advancing population and health studies. This pattern-based definition of the urban context allows differentiating a range of urban environments deepening the understanding of spaces defined as place of residence in demographic and public health studies. Data and the applications context are drawn from a study area in southern Ghana.

2. Study area and methodology

2.1. Study area and period

Urbanization in Ghana is spreading at a faster pace than among most of its West African neighbors. The 2010 Census of Population and Housing revealed that more than half of the country's population resided in urban areas, a figure that the UN projects to reach three quarters by 2050. Ghana Statistical Service (GSS) estimates that population in the Greater Accra Metropolitan Area increased from under 1.5 million in 1984 to almost 3 million in 2000, and then to the 4 million mark in 2010. However, urbanization is taking place not only in the capital (Accra) and other major cities (especially Kumasi), but also in smaller settlements both close to and far away from cities (Moller-Jensen and Knudsen 2008).

Studies of land cover and land use change in Ghana have found that migration is linked to decreasing woodlands in northern Ghana (Pabi 2007, Braimoh 2004), that in the Western region the most predominant changes are linked to mining, farming, lumbering, fuel wood collection and urbanization (Kusimi 2008), and that in the Accra region urbanization is the major driver of landscape transformation (Yorke and Margai 2007). In the capital city of Accra, urban expansion was mapped between 1985 and 2002 with Landsat imagery, showing a fast and unplanned spread of the city into its hinterland (Møller-Jensen and Yankson 1994, Møller-Jensen, Kofie and Yankson 2005). Yeboah (2003) describes the emergence of higher-quality residential sprawl in the peri-urban and rural localities adjacent to Accra's metropolitan area.

The study area from which data are drawn for this analysis is located in southern Ghana, consisting of 18 districts, including all of the Greater Accra Region (which comprised 5 districts in 2000) and 13 adjacent districts in the Central, Eastern and Volta regions shown in figure 1.The coastal regions of Ghana have seen a steady increase in population growth as the capital city Accra attracts a steady flow of migrants in search for opportunities. Accra's metropolitan area alone saw its population double between the mid 1980's and the beginning of 2000, when the last census took place. The study period for this research is the early part of the decade starting in 2000. The study area includes Accra and Tema, and their metropolitan fringes, periphery and hinterland. The districts selected for this study stretch over portions of Accra's neighboring regions defined here as areas that will likely be influenced by urban sprawl and other effects from changes in Accra in the near future. It is composed of a diverse landscape ranging from purely rural to central city (i.e., core) urban.

The year 2000 was selected as the study period to coincide with the Ghanaian population and housing census which permitted drawing comparisons between the landscape pattern based definition of the urban context and a range of demographic variables. All the analyzed and classified imagery was selected to match as closely as possible to 2000 time frame as was all the very high spatial resolution imagery used as reference data.

2.2. Methods

Urban context is characterized here using a uniform grid covering the study area through the use of satellite imagery and geographic information system (GIS) techniques. Landsat ETM + imagery was analyzed through spectral mixture analysis (SMA) and classified into Built and Vegetation land covers. Synthetic aperture radar imagery from the ERS-2 satellite was used to estimate a measure of radar backscatter texture and classified into a Built/Non Built land cover map. Landscape metrics are estimated for the SMA based Built and Vegetation land covers and combined with the radar texture based Built/Non Built map through a decision tree classifier in order to generate a classification of degree of urbanization (Figure 2)

2.2.1 Landsat imagery and processing—A cloud-free 30 m spatial resolution Landsat ETM+ terrain corrected image captured for path 193 and row 56 on 26 December 2002 was selected–he only cloud-free ETM+ image captured within the period 1999–2003. Pre-processing of the image consisted of masking waterbodies, sand flats and fire scars to

minimize the confusion of land cover classes. Spectral mixture analysis (SMA) was applied to the masked ETM+ image to estimate sub-pixel fractions of endmembers and the derived fraction images were used to generate a map of Built and land cover based on a hard (majority) classification.

The pre-processing of the Landsat ETM+ scene included applying waterbodies, sandbars and fire-scar masks. The waterbodies mask was extracted from a Land Use land Cover Map for 2000 digitized on Landsat Imagery by the Center for Remote Sensing and Geographic Information (CERSGIS) of the University of Ghana, Legon. The CERSGIS waterbodies layer included reservoirs, dams and rivers. In addition to the CERSGIS waterbodies layer an unsupervised classification was used to incorporate smaller lagoons and reservoirs that had been missed by the land use land cover map. The resulting improved waterbodies layer was manually edited to include salt ponds and wetlands by digitizing directly on the Landsat ETM+ scene and corroborating visually with Google Earth imagery. The Google Earth Imagery used to verify added water features include pansharpened Landsat (15m), Spot 5 (2.5m) and DigitalGlobe QuickBird 2 (65 cm) that correspond to the most current available dates. Atmospheric correction was considered unnecessary given that a single date Landsat image was classified based on signatures derived from the same image (Song et al. 2001).

Given the spectral similarity of bright sand bars and impervious surfaces, the decision was made to mask out sand flats in order to reduce confusion between the two land cover classes. Bright sand flats were digitized on Google Earth using the most current available very high spatial resolution imagery which includes Pansharpened QuickBird 2, Spot 5. We assumed that sand flats are unlikely to have converted from built or vegetated land cover, which led us to decide to use the most current very high spatial resolution imagery available. A fire scar mask was also created to remove areas of savanna vegetation burned immediately prior to the image acquisition date, to avoid confusion with the dark (shade) endmember. The fire scar mask was created using a supervised classification of a principal components transformed image (Hudak and Brockett 2004).

The resulting masked image of digital number (DN) values for six (all multispectral except thermal infrared) wavebands was analyzed using spectral mixture analysis (SMA). SMA extracts sub-pixel information by assuming that the spectral reflectance of a pixel is the product of the linear combination of the spectra of pure components or endmembers (Lu and Weng 2008). Even though SMA was originally developed to classify natural environments (Adams, Smith and Gillespie 1993, Roberts et al. 1998), the technique was adapted to urban landscapes by Ridd (1995) to represent the land cover of Salt Lake City as a combination of vegetation, impervious surface and soil (VIS). The pixel un-mixing algorithm constrains the resulting fractions to sum to 1 for each pixel while each individual fraction is non-negative (Phinn et al. 2002), as is described in the following equation:

$$R_{i\lambda} = \sum_{m=1}^{M} f_{mi} r_{m\lambda} + \varepsilon_{i\lambda} \text{ and } \sum_{m=1}^{M} f_{mi} = 1, f_{mi} \geq 0 \quad \text{Eq. 1}$$

where spectral mixture $R_{i\lambda}$ is modeled at location as the sum of the fractions f_{mi} of M image end-members $r_{m\lambda}$ plus a residual $\varepsilon_{i\lambda}$ at waveband λ. In addition to estimating fractions for

each end-member the model generates a root-mean-square error (RMS) image that assesses the model fit as described in the following equation:

$$RMS = \sqrt{\frac{\left(\sum_1^N (\varepsilon_{i\lambda})^2\right)}{N-1}} \quad \text{Eq. 2}$$

where N is the number of bands and $\varepsilon_{i\lambda}$ is a residual term calculated for all pixels at waveband λ.

The accuracy of the proportions generated by SMA depends on the selection of spectral end-members used to represent pure classes in the un-mixing process. End-member spectra collected directly from the imagery were supported by a pixel purity index (PPI) (Phinn et al. 2002, Rashed et al. 2003) which ranks pixel values based on how often they are repeated in the extremes of the spectral distribution of the image (Boardman, Kruse and Green 1995). Candidate pixels were visually inspected on the pan-sharpened (15 m) scene and on very high spatial resolution satellite images in Google Earth (Pansharpened QuickBird 2 (0.7 m). Given the lack of very high spatial resolution imagery matching the date of the Landsat ETM+ scene (only 2% of the study area), the decision was made to expand the time frame for the reference imagery to cover 1998 to 2004 (27% of the study area) (Figure 3).

SMA models were run on different sets of candidate end-members and the resulting fractions and RMS images were evaluated for goodness of fit. Models producing fractions between 0 and 1 and maximum RMS error under a threshold were considered good models. Models that didn't fit those parameters had their end-member refined in an iterative process until the optimum set of end-members was identified. The final end-member selection consisted of five pure signatures, one for green vegetation (pixels selected from forested areas), non-photosynthetic vegetation (pixels selected from savannah areas), soil (pixels selected from patches of bare soil or dirt), impervious surface (pixels selected from built patches) and shade (pixels selected from areas in the shadows of ridges) (Figure 4).

The resulting Landsat-derived SMA fractions were input to a series of discrete threshold classifiers to identify and map Vegetation and Built land cover classes. ETM+ pixels with more than fifty percent impervious surface were classified as Built land cover. The land cover proportions resulting from the SMA showed that within urban areas shade played an important role in capturing building shadows and dark pavement. In order to capture shadows and dark pavement cover, contextual information was used to enhance a threshold classifier. Large settlements were delineated through visual inspection of the pan-sharpened (15 meter) Landsat ETM+ image, and pixels found within those areas with proportions of over fifty percent shade and twenty five percent impervious surfaces were also classified as Built. Pixels modeled as having more than fifty percent vegetation were classified as Vegetation cover. Results from the SMA confirm previous research identifying that shade is also largely associated with vegetated areas where trees cast and contain substantial amounts of shade (Lu, Moran and Batistella 2003). A normalized difference vegetation index (NDVI) was calculated from ETM+ wavebands 3 and 4, and compared to the proportions of

vegetation and shade produced by the SMA, confirming the overlap of vegetation and shade in more heavily vegetated areas. In order to capture the portion of shade found within the vegetation cover, pixels with more than 50% shade and 25% vegetation cover were also classified as Vegetation. The resulting classification product is a 30 m raster land cover map of the study area containing Built, Vegetation and Other land cover classes.

2.2.3 SAR imagery and processing—While optical sensors are limited by lack of transmission of short to medium wavelength electromagnetic energy through clouds and precipitation, synthetic aperture radar (SAR) sensors are capable of transmitting and receiving microwave energy that is sensitive to physical characteristics of land surfaces such as roughness, morphology and geometry in most atmospheric conditions (Soergel 2010). Applications of SAR imagery for urban and built area mapping have proven to be very effective, given the high return characteristic of man-made features (Haack and Bechdol 2000).

ERS-2 radar imagery collected in the C band (5.6 cm) with 12.5 m spatial resolution was acquired for the study area from the European Space Agency for three orbits: 18370 collected on October 25 1998; 19601 collected on January 19 1999; and 41373 collected on March 20 2003. Pre-processing and processing of the radar imagery was conducted for each orbital pass separately. Pre-processing involved applying a terrain correction algorithm and a speckle reduction filter while the processing included the estimation of a measure of texture that is then classified as Built or Non-Built land cover.

Ground range images were pre-processed using the NEST toolbox developed by the European Space Agency (Engdahl et al. 2012). A range Doppler terrain correction algorithm was implemented for terrain correction and radiometric normalization, using a 30 m spatial resolution Global Digital Elevation Model (GDEM V2) derived from the Advanced Spaceborne Thermal Emission and Reflection Radiometer (ASTER) satellite sensor and precise orbit files from the Delft Institute for Earth-Oriented Space Research. In addition, a SAR simulation for orthorectification was used to generate a layover mask. Adaptive filters are commonly used for speckle reduction in radar imagery because they have the capacity to reduce multiplicative noise (Lee et al. 1994). A refined Lee filter was used to reduce speckle noise generated by the interference of individual scatterers by examining variance in a 7×7 window and establishing a threshold that detects edges, (Lee et al. 2009). The terrain-corrected SAR image and layover mask were closely inspected against very high spatial resolution imagery on Google Earth and the DEM in order to verify that areas susceptible to terrain distortion were masked from subsequent processing. Research in settlement mapping has shown that radar imagery is particularly useful in areas with little terrain where background classes can be defined as flat undeveloped surfaces with low radar returns against which artificial structures with high returns easily stand up (Haack and Slonecker 1994). Through visual inspection, areas located at higher elevations were identified as irregular bare rock formations generating mixed returns and foreshortening distortions which appeared to be missed by the terrain correction and layover mask. After close examination of the radar backscatter against optical imagery, the decision was made to expand the layover mask in areas located above 200 m elevation using a 200 m buffer to remove any remaining foreshortening distortions. The expanded mask helps to ensure that the radar backscatter

captured by the sensor is only minimally influenced by the radar beam interacting with the terrain, and is largely a product of its interaction with man-made structures. Finally, the same waterbodies mask used for the Landsat scene was used to mask all water features, salt ponds and wetlands.

Researchers exploit the ability of radar imagery to detect structures and forms through the use of measures of texture. The use of texture extracted from radar imagery allows for the delineation of features and has been found to improve image classification of land cover and land use (Herold et al. 2004, Dell'Acqua and Gamba 2003, Dell'Acqua et al. 2006). Several measures of texture were tested on the filtered radar imagery and a 9×9 window was selected to estimate the standard deviation of the radar backscatter values within the moving window. The selection of the 9×9 pixels moving window was based on the assumption that an area of 112.5 m by 112.5 m roughly correspond to the size of a city block that would identify a significant cluster of buildings. The standard deviation texture image was then smoothed using a 3×3 pixel moving window in order to remove outliers. The resulting variance of radar backscatter was used as an indicator of spatial composition of the built environment, where heterogeneous returns are associated with complex artificial landscapes such as the man-made features characteristic of settlements. A GIS layer depicting settlement locations from Ghana Statistical Service was used in combination with very high spatial resolution imagery from Google Earth as reference to establish a threshold in the radar texture that maximizes the detection of populated areas. The three orbits processed independently were classified as Built/Non-built land covers based on the defined threshold of radar texture and then mosaicked into a single raster file covering the entire study area.

2.2.4 Landscape metrics of Built and Vegetation patches—Researchers studying urban form have found that landscape metrics of multi-class land cover land use maps derived from classified remotely sensed imagery efficiently portray the complexity of cities (Herold, Scepan and Clarke 2002, Luck and Wu 2002, Pesaresi and Bianchin 2003, Herold, Goldstein and Clarke 2003) and of smaller rural settlements (Wang and Caldas 2014). Studies focusing on capturing the morphological transition between urban and rural places have shown that patch density, mean patch size and patch size variability describe best how fragmented, dispersed and heterogeneous the built environment is (Luck and Wu 2002, Herold et al. 2003, Seto and Fragkias 2005).

To study urban structure with landscape metrics requires partitioning the city into homogenous units of analysis (Herold, Couclelis and Clarke 2005). This study uses a uniform grid cell approach to estimate landscape fragmentation throughout the study area. Six different cell sizes were tested, ranging from 450 m by 450 m to 14400 m by 14400 m. Our analysis of the resulting landscape metrics indicated that the smaller cells maximized the detection of heterogeneous landscape patterns. We concluded that cell sizes larger than 450 m by 450 m denigrated our ability to derive meaningful distinctions among the resulting classes, especially given the spatial resolution of the imagery available to us.

Class and landscape metrics were estimated for the SMA-based Built and Vegetation land cover classes for the 450 m grid that corresponds to a 15 by 15 pixel cell which is defined as the landscape unit of analysis. The degree of landscape fragmentation, dispersal and

complexity was studied by examining spatial patterns of Built and Vegetation patches within the 450 m cell along the urban transition.

The metrics were calculated using FRAGSTATS software (McGarigal and Marks 1995). Class metrics for the Built and Vegetation land cover classes included percent land cover, patch density, coefficient of variation of patch area and area weighted mean fractal dimension of patches. The heterogeneity of the patterns of Built and Vegetation land cover within each 450 m cell was quantified using percentage of land cover and density of patches for each land cover class according to the following equation:

$$\text{Patch Density} = \frac{n_i}{A}(10000) \qquad \text{Eq. 3}$$

where n_i is the number of patches of class i and A is the total area in m^2 which is then converted into density per 100 hectares.

The variability in patch sizes for the Built and Vegetation land covers was estimated for each 450 m cell with a coefficient of variation of patch area with the following equation:

$$\text{Patch size coefficient of variation} = \frac{\sqrt{\dfrac{\sum_{j=1}^{n}\left[a_{ij} - \left(\sum_{j=1}^{n} a_{ij}\right)\right]^2}{n_i}}}{\dfrac{\sum_{j=1}^{n} a_{ij}}{n_i}} \qquad \text{Eq. 4}$$

where a_{ji} is the area of patch ij of class i and n_i is the number of patches.

The complexity of the shapes of urban patches was assessed through estimates of area-weighted mean patch fractal dimension, which have shown to help differentiate between compact dense urban areas and the patchy urban fringe (Batty and Longley 1988, Mesev et al. 1995). Area weighted mean fractal dimension was estimated for Built and Vegetation patches within each 450 meter cell according to the following equation:

$$\text{Area weighted mean Fractal dimension} = \sum_{i=1}^{m}\sum_{j=1}^{n}\left(\frac{2\ln(0.25 p_{ij})}{\ln a_{ij}}\right)\left(\frac{a_{ij}}{TA}\right) \qquad \text{Eq. 5}$$

where a_{ji} is the area of patch ij (class i),p_{ij} is the perimeter of m number of classes (patch types) and TA is the total area.

In addition, an index of contagion was used to evaluate adjacency and compactness in the landscape, describing the spatial arrangement of different land covers within the landscape unit (Yeh and Huang 2009, Herold et al. 2003, Dietzel et al. 2005).

$$\text{Contagion Index} = \left[1 + \frac{\sum_{i=1}^{m} \sum_{k=1}^{m} p_i \left(\frac{g_{ik}}{\sum_{k=1}^{m} g_{ik}} \right) \left[\ln(p_i) \frac{(g_{ik})}{\sum_{k=1}^{m} g_{ik}} \right]}{2 \ln(m)} \right] \quad \text{Eq. 6}$$

where p_i is the proportion of the landscape that is occupied by patch type (class) i, g_{ik} is the number of adjacencies (joins) between pixels of patch types i and k based on the double count method and m is the number of patch types present in the landscape.

2.2.5 Defining the urban context—The fusion of optical and radar based land cover products provides an opportunity to improve the accuracy of the land cover classification obtained from individual sensors. The radar imagery was particularly useful to detect small settlements that were missed by the SMA-based approach on the optical imagery. A scheme is proposed to describe landscape patterns of the built and vegetation land covers that combines measures of landscape fragmentation extracted from the classification of optical imagery with a measure variability of the built class extracted from radar imagery. A nine-class scheme was created to describe in a rank-order categorical manner the continuous transition of the urban context. The scheme represents an urban gradient defined as: Compact urban core, Fragmented large urban patches, Dense and dispersed small urban patches, Fragmented sub-urban, Scattered settlements, Sparsely populated, Fragmented transition, Fragmented unsettled and Unsettled land (Figure 5).

The conceptualization of the nine class scheme is the product of the combination of measures of land cover fragmentation (SMA-based classification) with a measure of variability of the radar-based Built class through a series of rules. The rules were defined *a priori* by analyzing the frequency distributions of six measures of land cover fragmentation and the standard deviation of the radar-based Built variable, splitting each variable in two (high and low values) using a natural breaks classification scheme that minimizes within-class variance and maximizes between-class variance. The natural break split for each variable was used to define a series of consecutive rules where the resulting classes (Figure 6) were named and validated by examining a set of representative cells for each class against very high spatial resolution imagery on Google Earth.

Decision tree classifiers are non-parametric models that deal efficiently with numerical and categorical data, making them a suitable approach to classify urban context based on imagery extracted variables such as land cover and measures of texture and morphology from different data sources. A decision tree classifier was used to classify the 450 m cells or landscape units into one of nine urban context classes, using the measures of landscape fragmentation estimated on the SMA-based classification of Built and Vegetation land covers and the aggregated radar texture based Built cover. This classification technique takes advantage of the spectral characteristics of the optical imagery, the pattern characteristics of the landscape metrics, and the structural characteristics of the radar imagery to generate a range of urban context classes that describe the varying physical characteristics of the

landscape. Nine cell level measures of landscape fragmentation and the cell level classified radar texture were used as inputs for the decision tree classifier to generate the pattern based classification of the urban context.

The VIS based Built land cover class was used to stratify the study area into high percent Built, medium percent Built and low percent Built, clipped to the section of the study area covered by very high spatial resolution imagery on Google Earth between 1998 and 2004 and then overlaid to the 450 m uniform grid to draw a stratified random sample of 690 cells for training and validating the decision tree. Given that built land represents a very small portion of the study area, the more urban strata were oversampled in order to select a minimum of 60 cells per class. The reference cells were visually inspected on very high spatial resolution Google Earth imagery and assigned to one of the nine classes based on a series of rules describing the predominant land cover type within the cell and level of fragmentation of the land covers found within the cell (Table 1).

The 690 cells were visually inspected and assigned to one of the nine classes, and then were partitioned into training and testing samples for a C5.0 boosted tree (10 trials) to model urban context based on landscape and texture metrics. The boosted tree is an iterative process to improve on the previous tree and reduce the number of errors. A random sample of 349 of the reference cells were used to train the tree and the remaining 344 were used to validate the tree. The breaks produced by the boosted tree (Figure 7) are based on the input variables for the reference data.

2.2.6 Accuracy assessment—Accuracy of the Built and Vegetation land covers classified from Landsat-derived SMA fractions was assessed by comparing the land cover classification to very high spatial resolution imagery from Google Earth for the 2000–2004 timeframe for a random sample of 1000 points. The sample size was increased until a minimum of 50 points was reached for each of the classes (Congalton 1991). Accuracy of the Built/Non-Built classification based on radar texture was assessed by comparing it to very high spatial resolution imagery from Google Earth for the same time frame for an independent random sample of 900 points. The sample size was increased until a minimum of 50 points was reached for the Built class. Confusion matrices and overall agreement statistics were estimated for each of the classifications.

Accuracy of the urban context classification was assessed by comparing the manually classified 450 by 450 m cells from the validation portion of the reference data against classes predicted by the decision tree for the same sample, a confusion matrix and overall agreement statistics were calculated. The use of a confusion matrix identifies how much misclassification is taking place for each one of the classes but does not allow measuring the magnitude of the errors. Errors that could be considered minor arise when a continuous scale is converted into discrete categories and areas that are relatively similar are assigned to two different but contiguous classes (Foody 2002). Given the gradient nature of the urban context classification scheme, confusion of adjacent classes was expected to be substantial but not-problematic. A fuzzy measure of accuracy was used to differentiate minor and major misclassification errors in the urban context classification. An independent stratified random sample of 375 cells was selected, oversampling the most urban classes until a minimum of

30 cells was reached for each class. Following a linguistic scale developed by Woodcock and Gopal (2000), the predicted class for the sample of cells are evaluated in detail against very high spatial resolution Google Earth imagery and scored on a scale of 1 to 5, with 1 meaning absolutely wrong and 5 meaning absolutely right (Table 2). Cells that are scored as 1 or 2 are considered major errors while cells scored as 3 or 4 are considered minor errors and cells scored 5 are considered accurately classified.

3. Results

3.1 SMA based vegetation and built land cover map

The land cover map produced using SMA is depicted in Figure 8 a) and shows that there is very little separation between Accra and Tema, the two large and sprawling metropolitan areas that dominate the urban system in the region. A network of smaller settlements, such as the town of Agona Swedru (Figure 8 b and c), can be observed spreading east-west following the coastline and scattered mid-size towns extend inland following major roads.

An examination of the confusion matrix (Table 3) for the SMA-derived land cover map indicates a high overall agreement of 91%, with producer's and user's accuracies for both the Built and Vegetation land cover classes > 80%. The producer's accuracy indicates the probability that the reference pixels are accurately classified and represent a measure of omission errors while the user's accuracy indicates the probability that the classified pixels represent the right category on the ground and are a measure of commission error. The VIS-based Built class has a 15% omission error which indicates that the classification is successfully detecting most of the built environment while a 19% commission error points to a persistent level of confusion between the Built and Other land cover class.

Results from the final SMA model suggest that distinguishing soil and built land cover classes is challenging given the spectral similarity of both classes, and also because of the high prevalence of mixing that occurs in cities of the developing world where many of the streets remain unpaved (Ridd 1995, Powell and Roberts 2008), or where soil is deposited on paved street surfaces, especially as runoff after rainy periods.

3.2 SAR texture-based Built class

The resulting confusion matrix (Table 4) demonstrates that while the map of the Built class derived from SAR texture has a user's accuracy of 67 %, it has a much higher producer's accuracy of 94%. The low levels of omission error indicate that the radar texture-based measure of the built environment is successful at detecting the majority of manmade features in the study area, while the high commission error indicates that there is a fair amount of confusion between Built and Non-built classes.

Close visual inspection of the SMA-and radar texture-based maps of the Built land cover in conjunction with Google Earth imagery indicated that the radar texture-derived map captures Built features for a wider range of settlement sizes in the study area (Figure 9). The small towns of Kwame Adewe and Nsutapon on figure 9 b–d and e–g illustrate how the radar-based map is able to detect small towns that are missed by the SMA-based classification of the Built class. While the Built map extracted from SMA seems to have a fair amount of

omission, the radar texture-extracted Built class, given its finer spatial resolution and imaging mode, is capable of identifying much smaller towns.

3.3 Classification of the urban context

Landscape and class metrics estimated for the 450 m cells (58,000 cells covering the study area) described in the Methods section and a cell level standard deviation of the radar texture-based Built class were used as input for the decision tree classifier. The resulting classification combined the ten intermediate variables extracted from optical and radar imagery into a nine class urban context classification that describes the spatial composition of land cover throughout the urban transition.

The urban context classification map (Figure 10) identifies almost 870 (1.5%) out of the 58,000 cells as Compact urban areas. These cells are located mainly in Greater Accra and Tema, in the centers of cities such as Koforidua and Winneba, and within major coastal and inland settlements (Figure 10). Cells classified as Fragmented large urban patches compose 1.3% of the study area and are mostly located within the central areas of major cities and settlements. A similar number of cells is identified as Dense and dispersed small urban patches and are found closer to the outskirts of larger cities such as the area located between Accra and Tema. The Fragmented sub-urban class is restricted to the outskirts of large cities found almost entirely in coastal areas, where urbanization is spreading at a fast pace. Scattered settlements covering 0.8% of the study area, on the other hand, are spread around the periphery of intermediate towns, most of them inland. Cells classified as sparsely populated areas cover 1295 cells (2.2%) and are scattered throughout the study area extending beyond the peripheries of consolidated towns. Finally, cells identified as transitional classes spread into unsettled land following a band pattern that expands beyond the periphery of settled areas.

The confusion matrix (Table 5) indicates an overall agreement of 77%; it is evident that user's accuracy is lower than producer's accuracy. The highest omission errors were found both on the least urban and most urban classes in the Fragmented transition and Fragmented large urban patches classes. High commission errors are found on the most and least urban classes, as indicated by figure 10. The most urban of the context classes (e.g., Compact urban and Fragmented large urban patches classes), exhibit a fair amount of confusion while the more rural Fragmented unsettled land and Fragmented transition classes show some confusion. The matrix and figure 11 indicate that while there is some confusion between similar classes (i.e., adjacent classes in a rank-order sense), the automated classification of urban context classes shows close agreement with the reference data derived from the visual interpretation of very high spatial resolution imagery.

Results from the fuzzy accuracy assessment indicate a high degree of correspondence when using a score of agreement with the reference data. The right class column on table 6 includes scores 1 to 3 corresponding to "absolutely right," "good answer" and "reasonable answer," while the exact class only captures score 1-absolutely right. The average agreement between classification and reference data improved from 61% to 87% when using the right class over the exact class. Given the continuous nature of the classification scheme, the use of a broader definition of agreement appears to be an appropriate way of assessing accuracy.

The improvements in agreement levels through the use of the fuzzy accuracy approach indicate that there is notable overlap between adjacent classes, an artifact of the gradient approach.

4. Discussion and Conclusions

Rapid urbanization is reshaping the morphology and function of cities globally. By portraying rural and urban areas as clearly distinct spaces, dichotomous rural/urban classifications ignore the importance of flows of people and products that connect these spaces and belie how urban processes are remaking global landscapes far beyond urban areas. In this paper, we have created and evaluated an urban context classification scheme that attempts to characterize different urban contexts that exist along a gradient between the arbitrary extremes of urban and rural. We demonstrate a novel characterization of the urban context based exclusively on the pattern characteristics of land cover distributions. A series of landscape metrics were computed for Built and Vegetated land cover maps with the goal of differentiating areas based on the degree of landscape fragmentation.

Two intermediate and independent land cover classifications were generated and then integrated, based on our analysis of optical and radar imagery it is evident that each of the approaches has advantages and limitations. The workflow for the processing of the optical imagery estimates sub-pixel proportions of land cover and then classifies them into discrete land cover classes in order to generate distinct land cover patches that are further analyzed through landscape metrics. Even though the classification of the Landsat-derived SMA fractions leads to a significant loss of sub-pixel land cover detail, the categorical product allows for the analysis of spatial patterns of land cover patches that would not be possible to achieve with more continuous spatial data. Results from the accuracy assessment for the SMA based classification of land cover indicate that there is a fair amount of omission, meaning that we are missing some built and vegetation patches, most likely because of their smaller proportions within the 30 m pixel. On the other hand, the radar-based classification had higher commission errors, meaning that there is at least some confusion between the Built and Non-Built classes using just that method. By combining the SMA-and radar-based land cover classes the attempt was made to overcome the limitations of each independent classification and generate a more accurate depiction of the built environment in the study area.

Patterns of land cover fragmentation were estimated using a 15 pixel by 15 pixel landscape unit to assess heterogeneity and complexity in patch sizes, and dispersion and interspersion of the land cover. This analysis provides an in-depth portrayal of the spatial patterns of land cover found within the study area. The generated urban context map with a spatial resolution of 450 m does not identify individual objects or land cover classes but it categorizes the landscape based on their spatial patterns following a gradient approach. The assumption in our method is that as city or settlement centers become more densely urbanized the built environment becomes more compact, whereas towards the outskirts of the city the land cover conversion brought by urban expansion means higher fragmentation and dispersion. The pattern-based urban context definition is based on the relative fragmentation of both the built environment and the vegetation land cover. A compact urban core bounds the most

urbanized end of the spectrum, with a predominant Built land cover class and very low levels of landscape fragmentation. As distance from the compact urban core increases, the built environment becomes increasingly fragmented giving way to dispersion and interspersion of Vegetation and Built land covers.

At distances from the city center reaching beyond the city limits, the landscape changes to scattered settlements and sparsely populated areas; fragmentation of the built environment peaks and is gradually replaced by areas transitioning from their natural state into cleared spaces suggestive of potential settlement. At the least urbanized end of the spectrum, unsettled lands are identified by lower levels of fragmentation in the vegetation land cover, while in transitioning spaces we begin to observe clearings linked to growing vegetation cover fragmentation. The pattern-based definition of the urban context used in this study captures a wider range of urban environments than do traditional rural/urban classifications. By differentiating the compact urban city center from highly fragmented suburban areas and scattered settlements, the urban context definition identifies important pattern differences among inhabited spaces. This study proposes defining urban context based on characteristics of landscape fragmentation, an approach that is easily replicable in other data poor countries. At the same time, it is important to recognize that the urban context classification derived in this study is a relative measure of degree of urbanization that is based on the fragmentation characteristics of this particular landscape. Its replicability in different geographic settings is a subject for future research.

The pattern based scheme was developed solely on the basis of imagery; the test of its utility lies in its ability to differentiate socioeconomic characteristics derived from independent sources. While a complete test of its utility remains beyond the scope of this paper, the urban context classification was compared to census data summarized at the enumeration area (EA) level (average size 13 Km^2). A random sample of 2000 EAs was selected from a total of 5000 covering the study area and was categorized based on the predominant urban context class covering each sampled EA (i.e. the class that covers the majority of the EA). EA level measures of population density and percentage of population occupied in agriculture were estimated and examined against the EA's predominant urban context class. Results indicate that the highest percentages of population employed in agriculture are concentrated at the most rural end of the spectrum for scattered settlements, sparsely populated, fragmented transition, fragmented unsettled and unsettled land (Figure 12). It is interesting to note that the compact urban core has a higher percentage of population employed in agriculture than the fragmented sub-urban class, a result that would seem unlikely at first sight. However it is also worth pointing out that even though the compact urban core class captures the dense city center of Accra and Tema it also captures dense and compact city centers of intermediate cities and major towns. In those smaller cities the proportion of population working in agriculture is much higher than in sub-urban areas which are only concentrated around Accra. On the other hand, population density is highest in the most urban end of the spectrum for the compact urban core, fragmented large urban patches, and dense and disperse small urban patches classes and decreases significantly with the transition into the unsettled end of the scheme (Figure 13).

In our follow-on research, we are examining demographic trends throughout the range of urban contexts, to see if they provide clues as to where we can expect urbanization to spread in the future. It is our expectation that any research uncovering a rural-urban differential in demographic behavior or trends will be better understood when the urban gradient is taken into account. Although our preliminary results confirm that demographic patterns vary throughout the urban context, the pattern-based definition of the urban context remains an arbitrary definition of space. There is no consensus on what constitutes an urban place and that means that there will continue to be many ways of characterizing urban spaces. This study proposes a definition of urban context based on landscape fragmentation characteristics, an easily replicable approach in data poor environments. At the same time, it is important to recognize that the urban context classification derived in this study is a relative measure of degree of urbanization that is based on the fragmentation characteristics of this particular landscape. We encourage other researchers to test its replicability in different geographic settings.

By examining landscape pattern characteristics, this study suggests that urban mapping can be advanced beyond the traditional rural/urban or land cover and land use classifications towards the detection and inclusion of diverse urban environments. This study attempts to explain differences between rural and urban environments in developing countries where the fast pace of urbanization is generating dynamic landscapes. Further research is necessary to expand the understanding of how the urban context is linked to demographic patterns and more specifically to elucidate how emerging developing world urban environments are connected to population growth.

Acknowledgments

References

Adams JB, Smith MO, Gillespie AR. Imaging spectroscopy: Interpretation based on spectral mixture analysis. Remote Geochemical Analysis Elemental and Mineralogical Composition. 1993; 7:145–166.

Antrop M. Landscape change and the urbanization process in Europe. Landscape and Urban Planning. 2004; 67:9–26.

Batty M, Longley PA. The morphology of urban land use. Environment and Planning B: Planning and Design. 1988; 15:461–488.

Boardman, JW.; Kruse, FA.; Green, RO. Mapping target signatures via partial unmixing of AVIRIS data. Citeseer; 1995. 95-1

Braimoh AK. Seasonal migration and land use change in Ghana. Land Degradation & Development. 2004; 15:37–47.

Breuste J, Niemelä J, Snep R. Applying landscape ecological principles in urban environments. Landscape Ecology. 2008; 23:1139–1142.

Cadenasso ML, Pickett STA, Schwarz K. Spatial heterogeneity in urban ecosystems: reconceptualizing land cover and a framework for classification. Frontiers in Ecology and the Environment. 2007; 5:80–88.

Champion, AG.; Hugo, G. New forms of urbanization: Beyond the urban-rural dichotomy. Ashgate Pub Ltd; 2004.

Congalton RG. A review of assessing the accuracy of classifications of remotely sensed data. Remote Sensing of Environment. 1991; 37:35–46.

DeFries R, Asner GP, Foley J. A glimpse out the window: What landscapes reveal about livelihoods, land use, and environmental consequences. Environment. 2006; 48:22–36.

Dell'Acqua F, Gamba P. Texture-based characterization of urban environments on satellite SAR images. Geoscience and Remote Sensing, IEEE Transactions on. 2003; 41:153–159.

Dell'Acqua, F.; Stasolla, M.; Gamba, P. Unstructured human settlement mapping with SAR sensors. IEEE; 2006. p. 3619-3622.

Dietzel C, Herold M, Hemphill JJ, Clarke KC. Spatio - temporal dynamics in California's Central Valley: Empirical links to urban theory. International Journal of Geographical Information Science. 2005; 19:175–195.

Elvidge CD, Sutton PC, Wagner TW, Ryzner R, Vogelmann JE, Goetz SJ, Smith AJ, Jantz C, Seto KC, Imhoff ML. Urbanization. Land Change Science. 2004:315–328.

Engdahl, M.; Minchella, A.; Marinkovic, P.; Veci, L.; Lu, J. Geoscience and Remote Sensing Symposium (IGARSS), 2012 IEEE International. IEEE; 2012. Nest: An esa open source toolbox for scientific exploitation of sar data; p. 5322-5324.

Foody GM. Status of land cover classification accuracy assessment. Remote Sensing of Environment. 2002; 80:185–201.

Haack B, Bechdol M. Integrating multisensor data and RADAR texture measures for land cover mapping. Computers & Geosciences. 2000; 26:411–421.

Haack BN, Slonecker ET. Merged spaceborne radar and Thematic Mapper digital data for locating villages in Sudan. PE & RS-Photogrammetric Engineering & Remote Sensing. 1994; 60:1253–1257.

Haack BN, Solomon EK, Bechdol MA, Herold ND. Radar and optical data comparison/integration for urban delineation: a case study. Photogrammetric engineering and remote sensing. 2002; 68:1289–1296.

Harris RJ, Longley PA. New data and approaches for urban analysis: modelling residential densities. Transactions in GIS. 2002; 4:217–234.

Herold M, Couclelis H, Clarke KC. The role of spatial metrics in the analysis and modeling of urban land use change. Computers, environment and urban systems. 2005; 29:369–399.

Herold M, Goldstein NC, Clarke KC. The spatiotemporal form of urban growth: measurement, analysis and modeling. Remote Sensing of Environment. 2003; 86:286–302.

Herold M, Scepan J, Clarke KC. The use of remote sensing and landscape metrics to describe structures and changes in urban land uses. Environment and Planning A. 2002; 34:1443–1458.

Herold ND, Haack BN, Solomon E. An evaluation of radar texture for land use/cover extraction in varied landscapes. International journal of applied earth observation and geoinformation. 2004; 5:113–128.

Hudak AT, Brockett BH. Mapping fire scars in a southern African savannah using Landsat imagery. International Journal of Remote Sensing. 2004; 25:3231–3243.

Hugo G, Champion A, Lattes A. Toward a new conceptualization of settlements for demography. Population and Development Review. 2003; 29:277–297.

Kühn I, Klotz S. Urbanization and homogenization – Comparing the floras of urban and rural areas in Germany. Biological Conservation. 2006; 127:292–300.

Kusimi JM. Assessing land use and land cover change in the Wassa West District of Ghana using remote sensing. GeoJournal. 2008; 71:249–259.

Lambin EF, Turner BL, Geist HJ, Agbola SB, Angelsen A, Bruce JW, Coomes OT, Dirzo R, Fischer G, Folke C. The causes of land-use and land-cover change: moving beyond the myths. Global environmental change. 2001; 11:261–269.

Lee J-S, Wen J-H, Ainsworth TL, Chen K-S, Chen AJ. Improved sigma filter for speckle filtering of SAR imagery. Geoscience and Remote Sensing, IEEE Transactions on. 2009; 47:202–213.

Lee JS, Jurkevich L, Dewaele P, Wambacq P, Oosterlinck A. Speckle filtering of synthetic aperture radar images: a review. Remote Sensing Reviews. 1994; 8:313–340.

Lee KN. An urbanizing world. State of the world 2007: Our urban future. 2007:3–22.

Liu X, Herold M. Of patterns and processes: Spatial metrics and geo-statistics in urban analysis. Integration of GIS and remote sensing. 2007:93.

Longley PA. Geographical information systems: will developments in urban remote sensing and GIS lead to "better"urban geography? Progress in Human Geography. 2002; 26:231.

Lu D, Moran E, Batistella M. Linear mixture model applied to Amazonian vegetation classification. Remote Sensing of Environment. 2003; 87:456–469.

Lu D, Weng Q. Use of impervious surface in urban land-use classification. Remote Sensing of Environment. 2006; 102:146–160.

Lu, D.; Weng, Q. Remote Sensing of Impervious Surfaces. CRC Press, Taylor & Francis Group; Boca Raton, FL, USA: 2008. Mapping urban impervious surfaces from medium and high spatial resolution multispectral imagery.

Luck M, Wu J. A gradient analysis of urban landscape pattern: a case study from the Phoenix metropolitan region, Arizona, USA. Landscape Ecology. 2002; 17:327–339.

McDonnell M, Hahs A. The use of gradient analysis studies in advancing our understanding of the ecology of urbanizing landscapes: current status and future directions. Landscape Ecology. 2008; 23:1143–1155.

McGarigal K, Marks M. Spatial pattern analysis program for quantifying landscape structure. Gen Tech Rep PNW-GTR-351 US Department of Agriculture, Forest Service, Pacific Northwest Research Station. 1995

Mesev TV, Longley PA, Batty M, Xie Y. Morphology from imagery: detecting and measuring the density of urban land use. Environment and Planning A. 1995; 27:759–759.

Moller-Jensen L, Knudsen M. Patterns of population change in Ghana (1984–2000): urbanization and frontier development. GeoJournal. 2008; 73:307–320.

Møller-Jensen L, Kofie RY, Yankson PW. Large-area urban growth observations— a hierarchical kernel approach based on image texture. Geografisk Tidsskrift-Danish Journal of Geography. 2005; 105:39–47.

Møller-Jensen L, Yankson P. Assessing the Land Cover change of Accra using Landsat-TM data. Geografisk Tidsskrift-Danish Journal of Geography. 1994; 94:21–25.

Pabi O. Understanding land-use/cover change process for land and environmental resources use management policy in Ghana. GeoJournal. 2007; 68:369–383.

Pesaresi, M.; Bianchin, A. Recognizing settlement structure using mathematical morphology and image texture. In: Donnay, JP.; Barnsley, MJ.; Longley, PA., editors. Remote Sensing and Urban Analysis: GISDATA 9. CRC Press; 2003. p. 46-60.

Phinn S, Stanford M, Scarth P, Murray AT, Shyy PT. Monitoring the composition of urban environments based on the vegetation-impervious surface-soil (VIS) model by subpixel analysis techniques. International Journal of Remote Sensing. 2002; 23:4131–4153.

Potere D, Schneider A, Angel S, Civco DL. Mapping urban areas on a global scale: which of the eight maps now available is more accurate? International Journal of Remote Sensing. 2009; 30:6531–6558.

Powell RL, Roberts DA. Characterizing variability of the urban physical environment for a suite of cities in Rondonia, Brazil. Earth Interactions. 2008; 12:1–32.

Pumain D. An evolutionary approach to settlement systems. New Forms of Urbanization: Beyond the Urban-Rural Dichotomy. 2004

Rashed T, Weeks JR, Roberts D, Rogan J, Powell R. Measuring the physical composition of urban morphology using multiple endmember spectral mixture models. Photogrammetric Engineering and Remote Sensing. 2003; 69:1011–1020.

Ridd MK. Exploring a VIS (vegetation-impervious surface-soil) model for urban ecosystem analysis through remote sensing: comparative anatomy for cities†. International Journal of Remote Sensing. 1995; 16:2165–2185.

Roberts DA, Gardner M, Church R, Ustin S, Scheer G, Green RO. Mapping Chaparral in the Santa Monica Mountains Using Multiple Endmember Spectral Mixture Models. Remote Sensing of Environment. 1998; 65:267–279.

Rogan J, Miller J, Stow D, Franklin J, Levien L, Fischer C. Land-cover change monitoring with classification trees using Landsat TM and ancillary data. Photogrammetric Engineering and Remote Sensing. 2003; 69:793–804.

Seto KC, Fragkias M. Quantifying spatiotemporal patterns of urban land-use change in four cities of China with time series landscape metrics. Landscape Ecology. 2005; 20:871–888.

Seto KC, Reenberg A, Boone CG, Fragkias M, Haase D, Langanke T, Marcotullio P, Munroe DK, Olah B, Simon D. Urban land teleconnections and sustainability. Proceedings of the National Academy of Sciences. 2012; 109:7687–7692.

Seto KC, Shepherd JM. Global urban land-use trends and climate impacts. Current Opinion in Environmental Sustainability. 2009; 1:89–95.

Small C. A global analysis of urban reflectance. International Journal of Remote Sensing. 2005; 26:661–681.

Soergel, U. Review of Radar Remote Sensing on Urban Areas. In: Soergel, U., editor. Radar Remote Sensing of Urban Areas. Springer; Netherlands: 2010. p. 1-47.

Song C, Woodcock CE, Seto KC, Lenney MP, Macomber SA. Classification and Change Detection Using Landsat TM Data: When and How to Correct Atmospheric Effects? Remote Sensing of Environment. 2001; 75:230–244.

Stasolla M, Gamba P. Semi-automated extraction of human settlement extent in HR SAR images. 2008

Tatem AJ, Noor AM, Hay SI. Defining approaches to settlement mapping for public health management in Kenya using medium spatial resolution satellite imagery. Remote Sensing of Environment. 2004; 93:42–52. [PubMed: 22581984]

Toit MJ, Cilliers SS. Aspects influencing the selection of representative urbanization measures to quantify urban–rural gradients. Landscape Ecology. 2011; 26:169–181.

United Nations Population Division. World Population Prospects: The 2012 Revision. New York: United Nations; 2012.

United Nations Population Division. World Urbanization Prospects: The 2014 Revision Population Database. United Nations Population Division, Department of Economic and Social Affairs; 2014.

Van de Voorde T, Jacquet W, Canters F. Mapping form and function in urban areas: An approach based on urban metrics and continuous impervious surface data. Landscape and Urban Planning. 2011; 102:143–155.

Wang C, Caldas MM. Fragmentation Patterns in Land Reform Settlements in the Brazilian Amazon. Society & Natural Resources. 2014; 27:742–758.

Weeks J, Larson D, Rashed T. Contrast or continuum? The creation and application of an urban gradient index using remotely sensed imagery and GIS. annual meeting of the population association of America, Minneapolis. 2003:1–44.

Weeks JR. The role of spatial analysis in demographic research. Spatially integrated social science. 2004:381–99.

Weeks JR, Larson D, Fugate D. Patterns of urban land use as assessed by satellite imagery: An application to Cairo, Egypt. Population, Land Use, and Environment: Research Directions. 2005:265–86.

Weng Y-C. Spatiotemporal changes of landscape pattern in response to urbanization. Landscape and Urban Planning. 2007; 81:341–353.

Wickham JD, O'Neill RV, Jones KB. Forest fragmentation as an economic indicator. Landscape Ecology. 2000; 15:171–179.

Woodcock CE, Gopal S. Fuzzy set theory and thematic maps: accuracy assessment and area estimation. International Journal of Geographical Information Science. 2000; 14:153–172.

Yang Q, Li J, Gan X, Zhang J, Yang F, Qian Y. Comparison of landscape patterns between metropolises and small-sized cities: a gradient analysis with changing grain size in Shanghai and Zhangjiagang, China. International Journal of Remote Sensing. 2011; 33:1446–1464.

Yeboah IEA. Demographic and housing aspects of structural adjustment and emerging urban form in Accra, Ghana. Africa Today. 2003; 50:107–119.

Yeh C-T, Huang S-L. Investigating spatiotemporal patterns of landscape diversity in response to urbanization. Landscape and Urban Planning. 2009; 93:151–162.

Yorke C, Margai FR. Monitoring Land Use Change in the Densu River Basin, Ghana Using GIS and Remote Sensing Methods. African Geographical Review. 2007; 26:87–111.

Zipperer WC, Wu J, Pouyat RV, Pickett STA. The application of ecological principles to urban and urbanizing landscapes. Ecological Applications. 2000; 10:685–688.

Highlights

- Urban context is mapped for population studies in the West African country of Ghana

- Landsat and ERS2-SAR imagery are used to classify Vegetation and Built land cover

- A pattern based definition of the urban context is created using landscape metrics
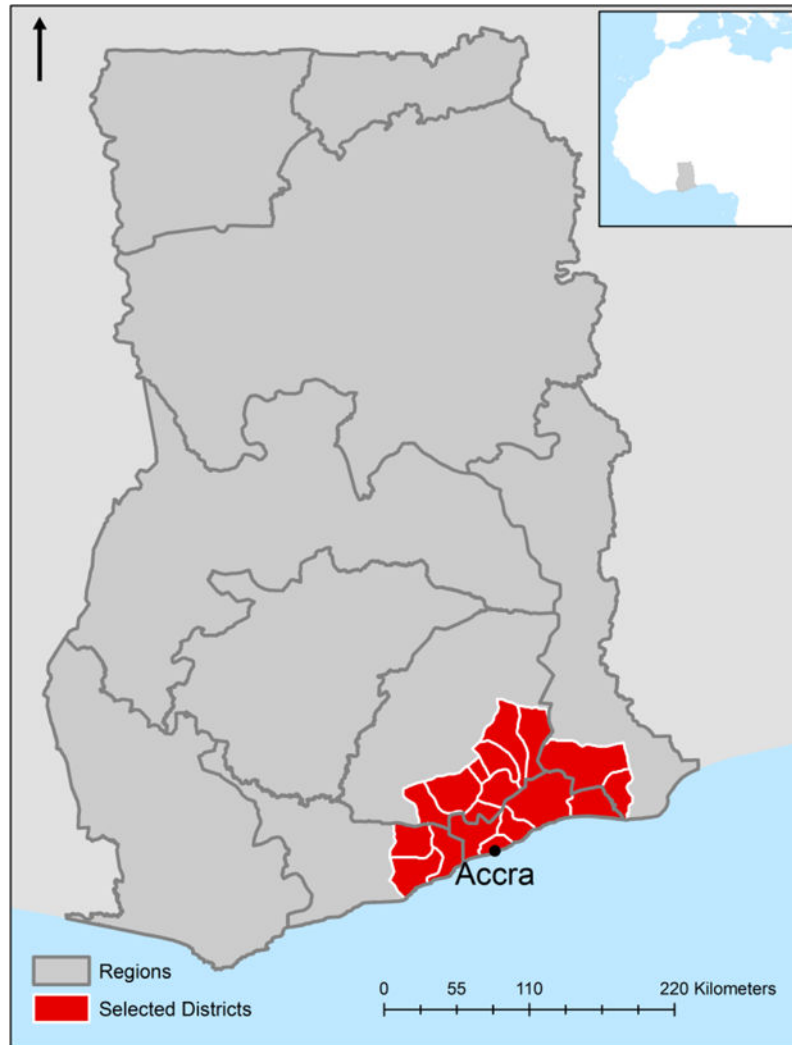
Figure 1.
Study area depicted in red within Ghana (gray) and the Gulf of Guinea in blue. Polygons within the study area represent census districts, while in the rest of Ghana represent regions (states).
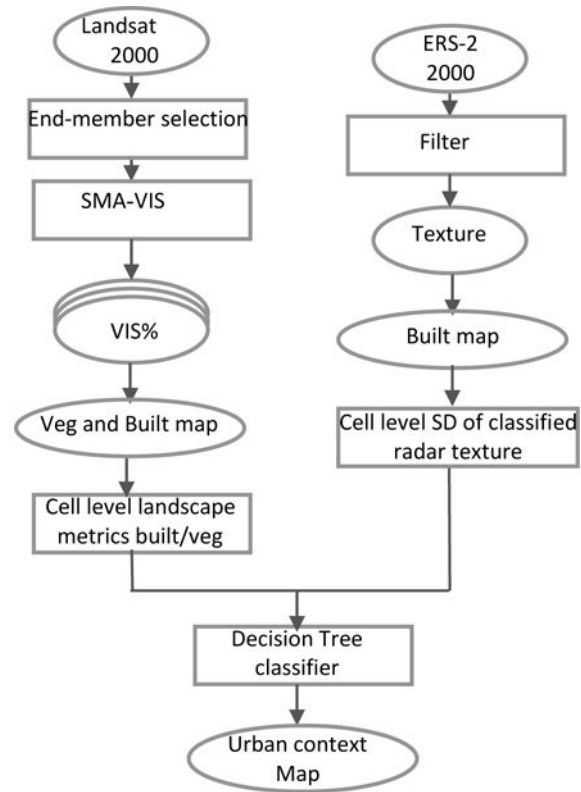
Figure 2.
Flow chart for urban context classification based on the combination of Landsat 2000 imagery and ERS-2 2000 imagery
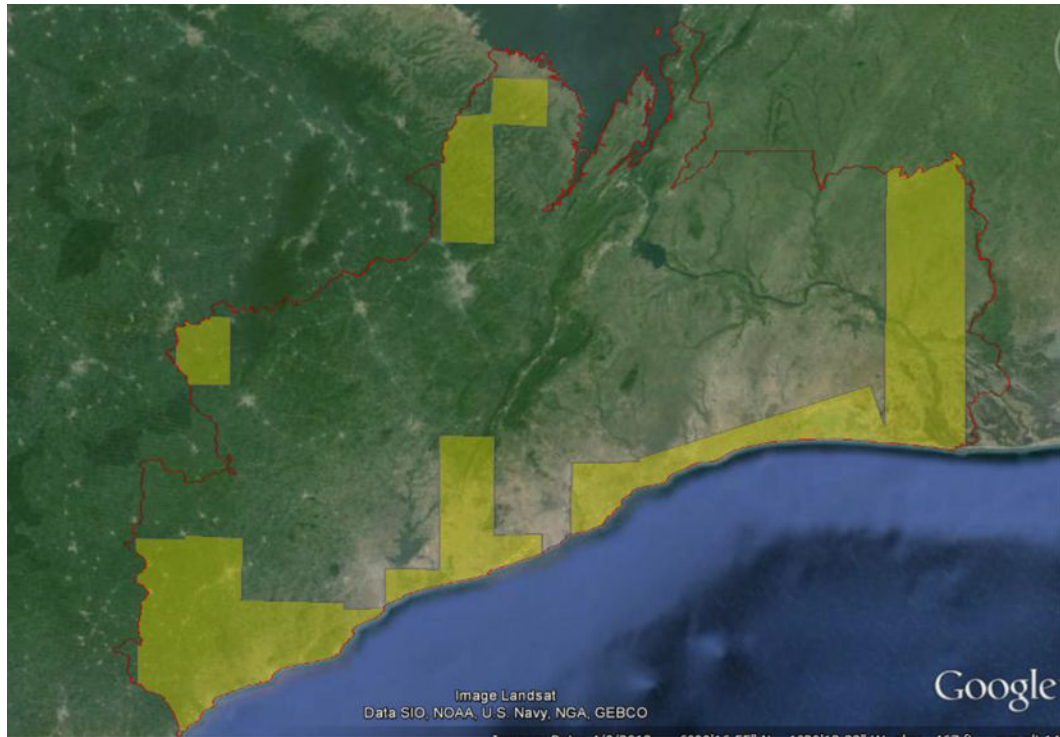
Figure 3.
Extent of the study area delineated with a red boundary on Google Earth and extent of the very high spatial resolution imagery available on Google Earth in the 1998 to 2004 time period. 27% of the study area is covered by very high spatial resolution imagery in the 1998–2004 time period.
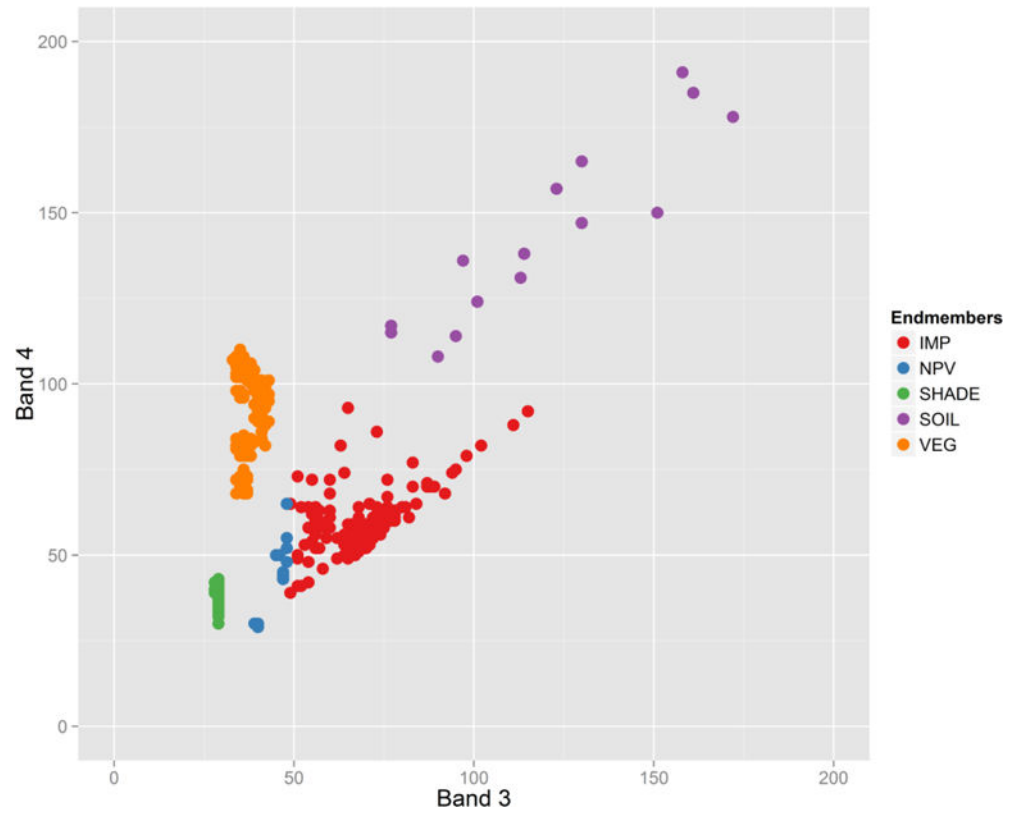
Figure 4.
DN values for endmembers selected using the pixel purity index for band 3 (red) vs band 4 (near infrared). Selected 5 end-members include Impervious surfaces, Non-photosynthetic vegetation, Shade, Soil and Vegetation.
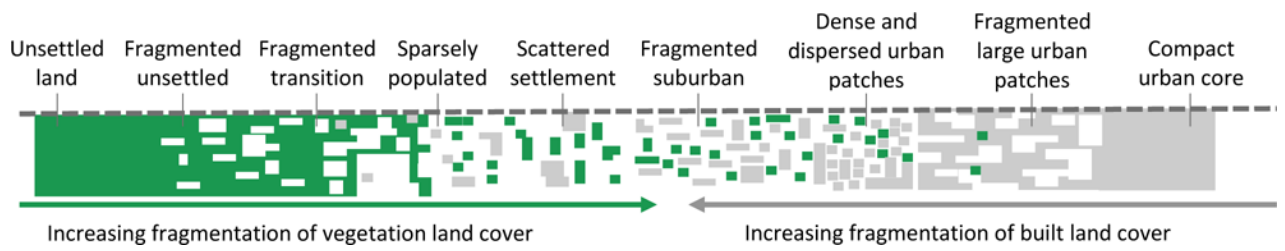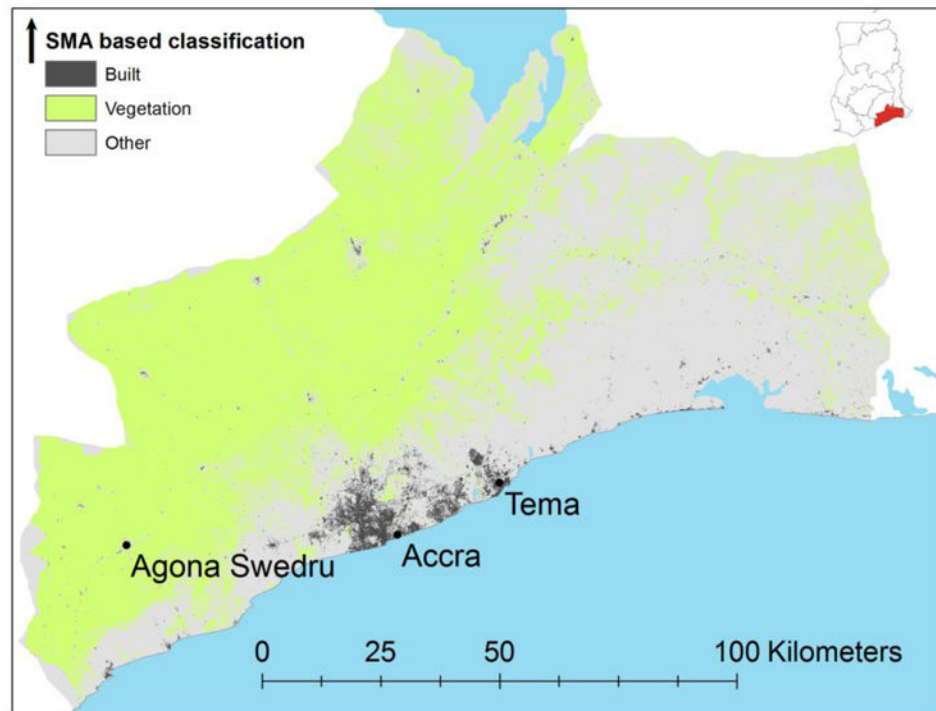
Figure 5.
Urban context classification scheme. On the most urban end compact and dense built land cover dominates, fragmentation increases in both built and vegetation land cover as classes transition towards rural environments. On the most rural end of the scheme compact and dense vegetation land cover dominates.
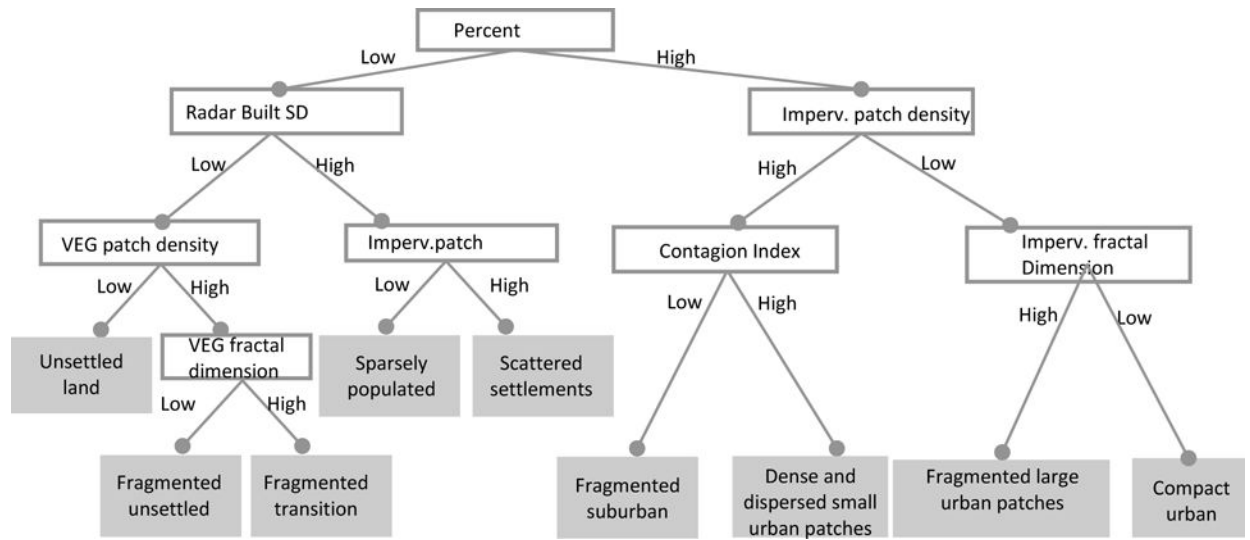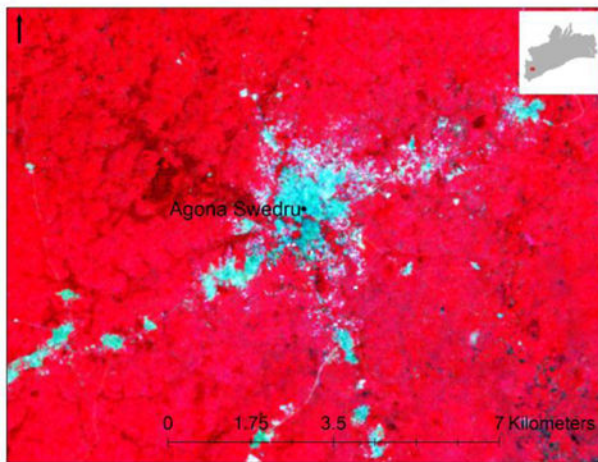
Figure 6.
Rules used to define the 9 class urban context classification scheme. Six measures of landscape fragmentation were analyzed and combined with an aggregated measure of radar texture to define the urban context classification scheme.
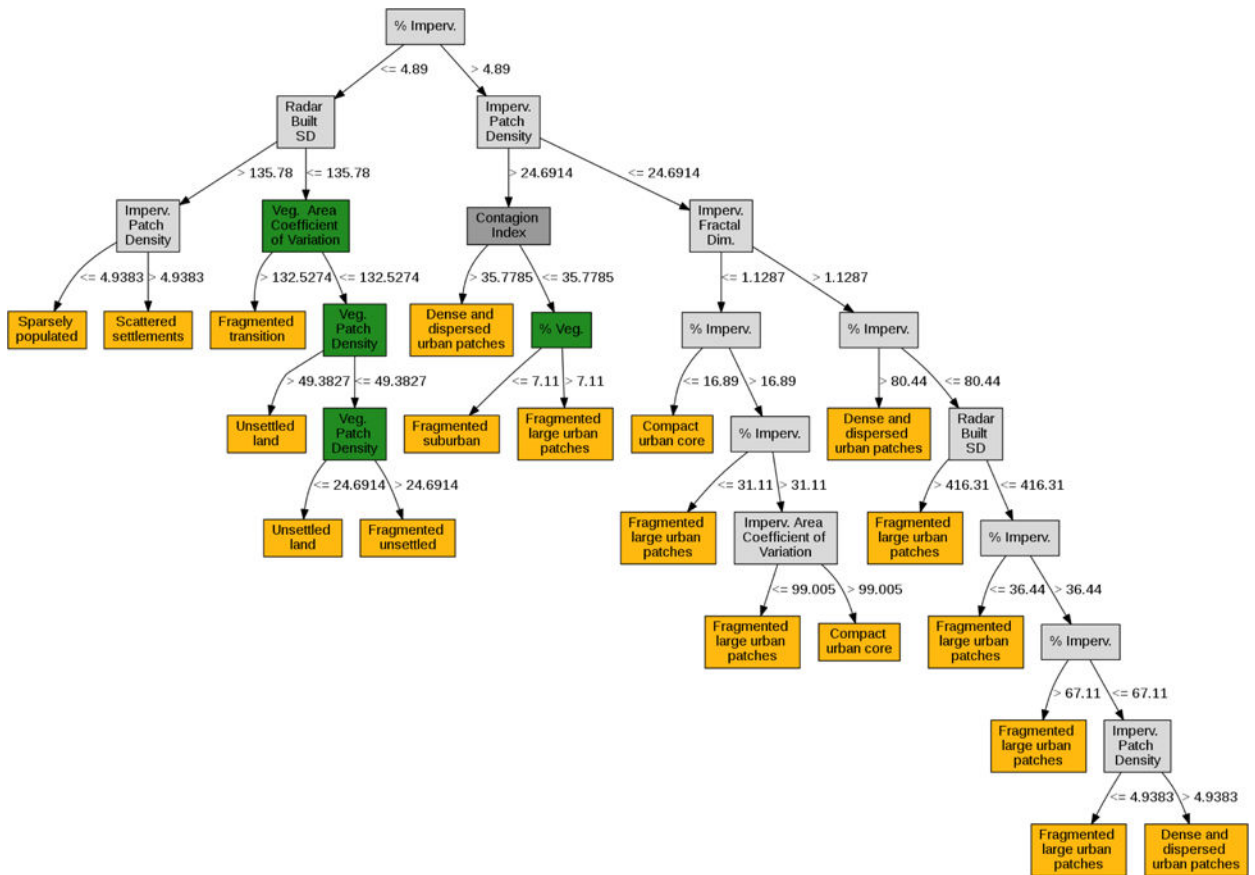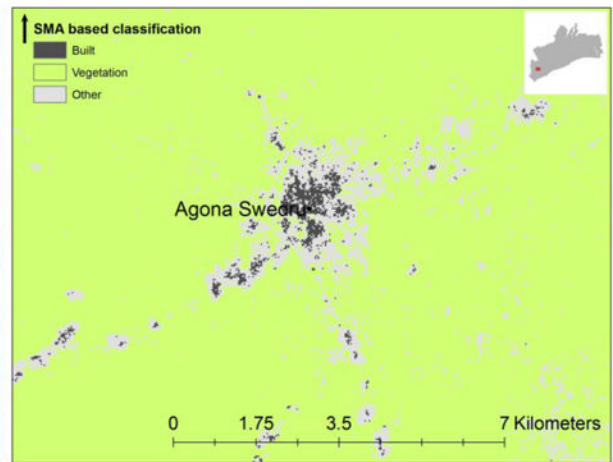
Figure 7.
Schematic illustrating C5.0 boosted tree (10 trials) input, classification split values and output. The yellow boxes indicate the classified urban context classes.
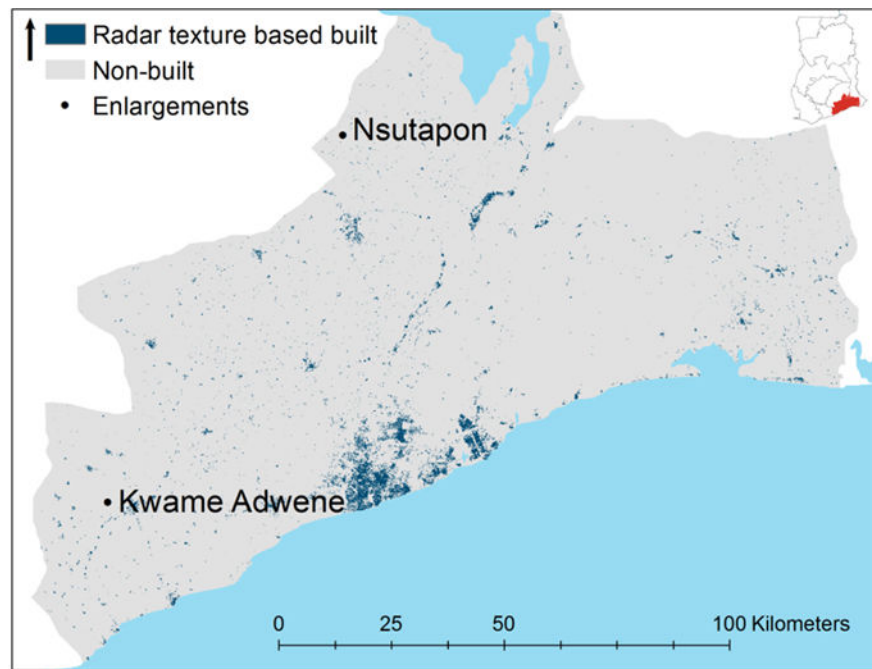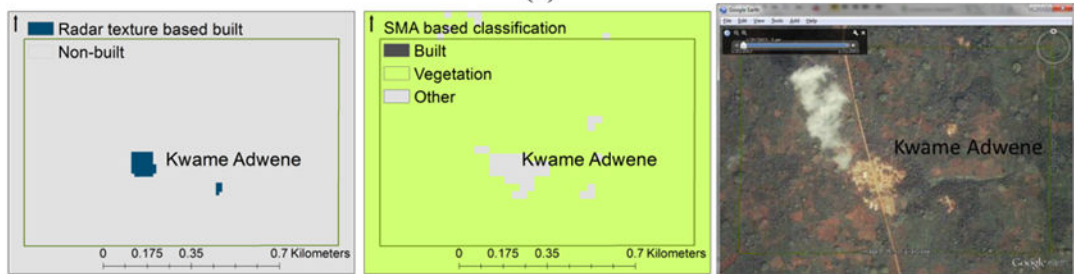
(a)

(b)

(c)

Figure 8.
(*a*) Built (>50% impervious & >25% impervious+>50% shade) and Vegetation (>50% vegetation & >25% vegetation+>50% shade) land cover extracted from SMA; (*b*) Landsat ETM+ false color infrared (bands 4-3-2) enlargement of the town of Agona Swedru (*c*) Built and Vegetation land cover extracted from SMA enlargement of the town of Agona Swedru.
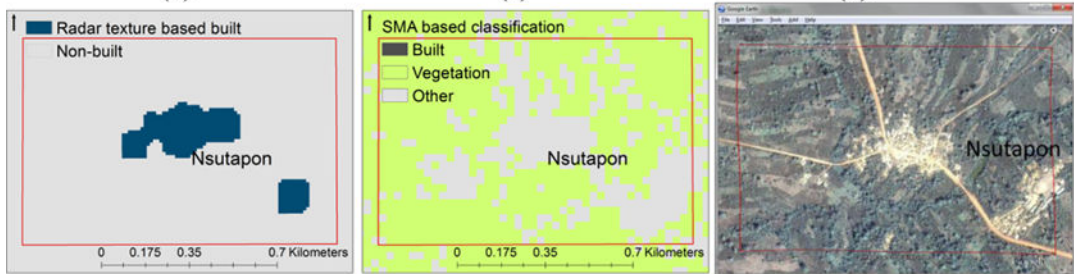
Figure 9.
(*a*) Radar-derived Built map; (*b*) enlargement of radar-derived Built map near the town of Kwame Adewe; (*c*) enlargement of SMA-based land cover map of the town of Kwame Adwene; (*d*) Google Earth image from the town of Kwame Adewene 2003; (e) Radar based built class zoom on the town of Nsutapon; (*f*) SMA based land cover classification zoom on the town of Nsutapon; and (*g*) Google Earth image from the town of Nsutapon 2000.
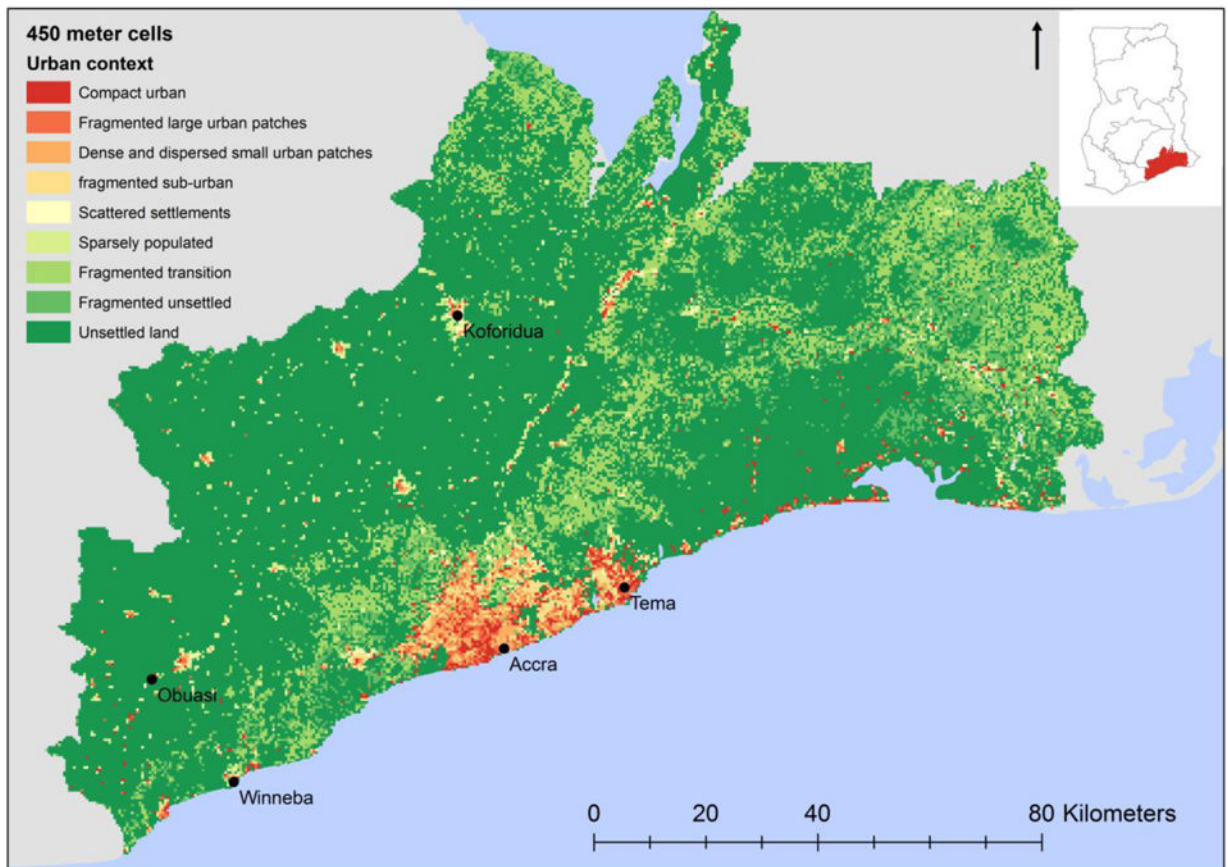
Figure 10.
450 meter cell urban context map. Accra, the capital city, and the port of Tema in the central coast are the two largest urban centers within the study area.
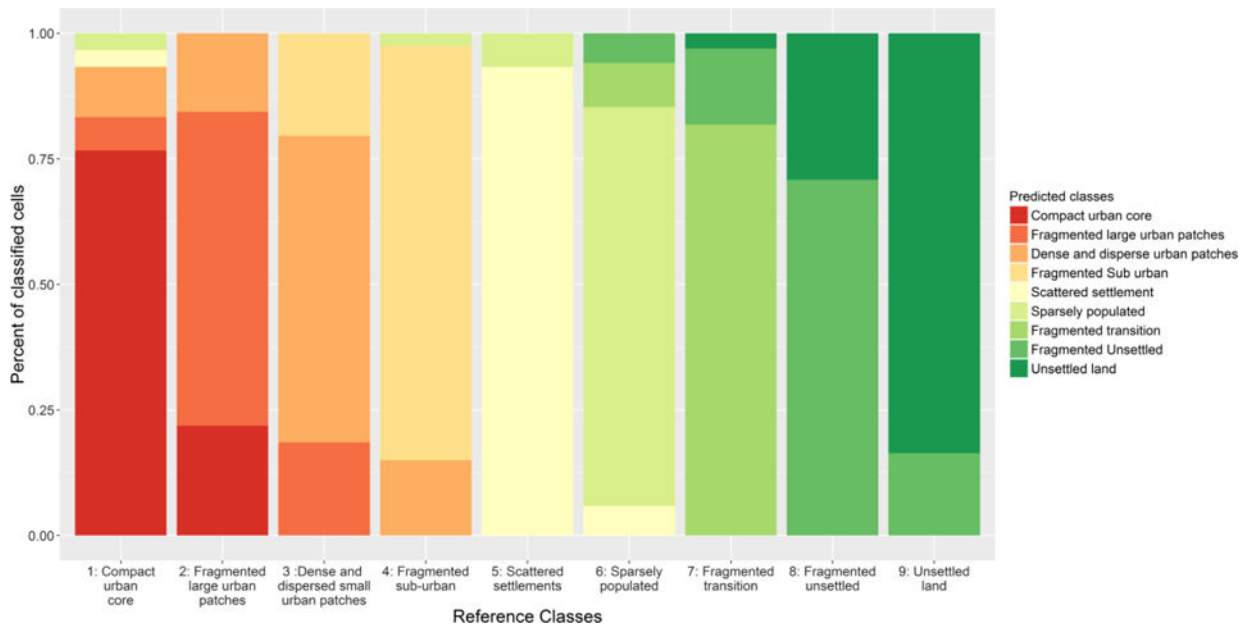
Figure 11.
Distribution of predicted versus reference classes. Commission error is present on both ends of the classification scheme. The dark red portion of the *Fragmented large urban patches* bar indicates confusion with the *Compact urban core* class. The dark green portion of the *Fragmented unsettled class* bar indicates confusion with the *Unsettled land class.*
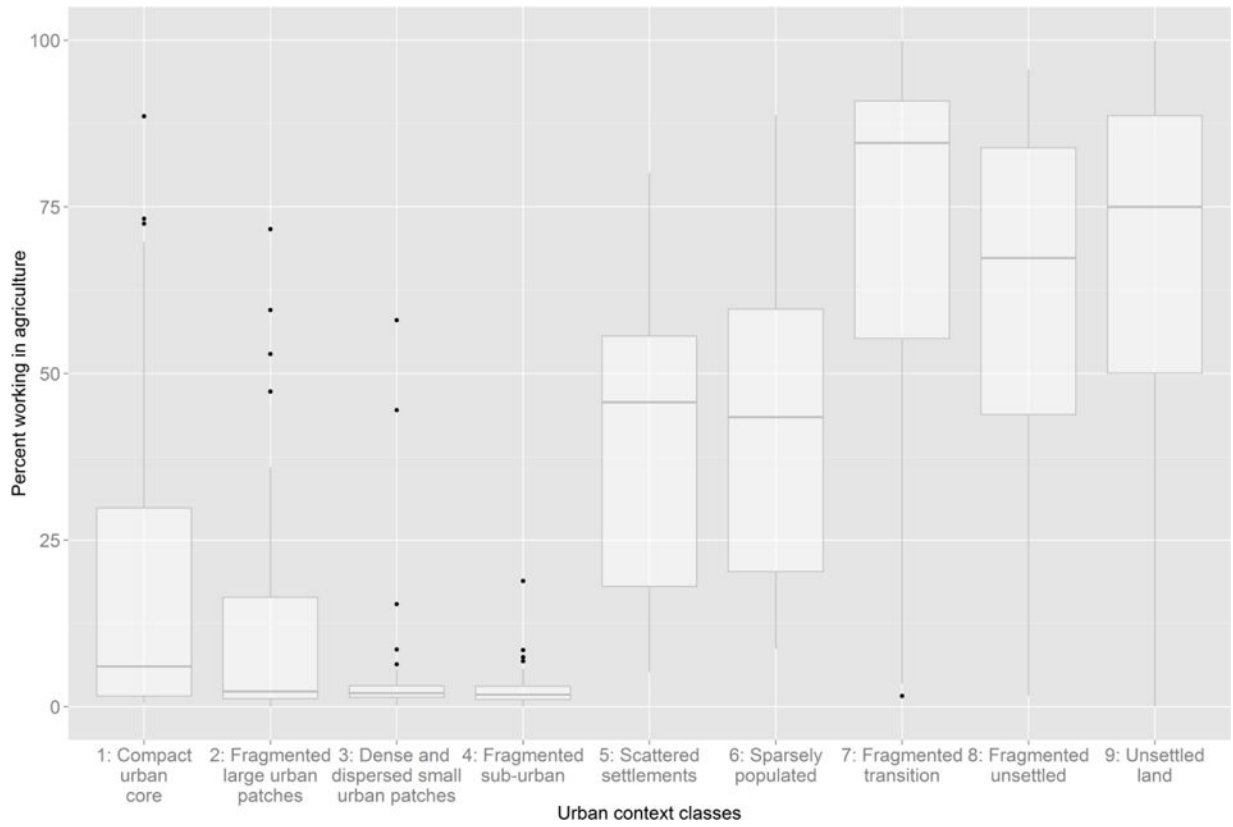
Figure 12.
Percent working in agriculture throughout the urban context classification. The highest percentage of population working in the agricultural sector is found on the most rural end of the scheme, Fragmented transition, fragmented unsettled and unsettled land.
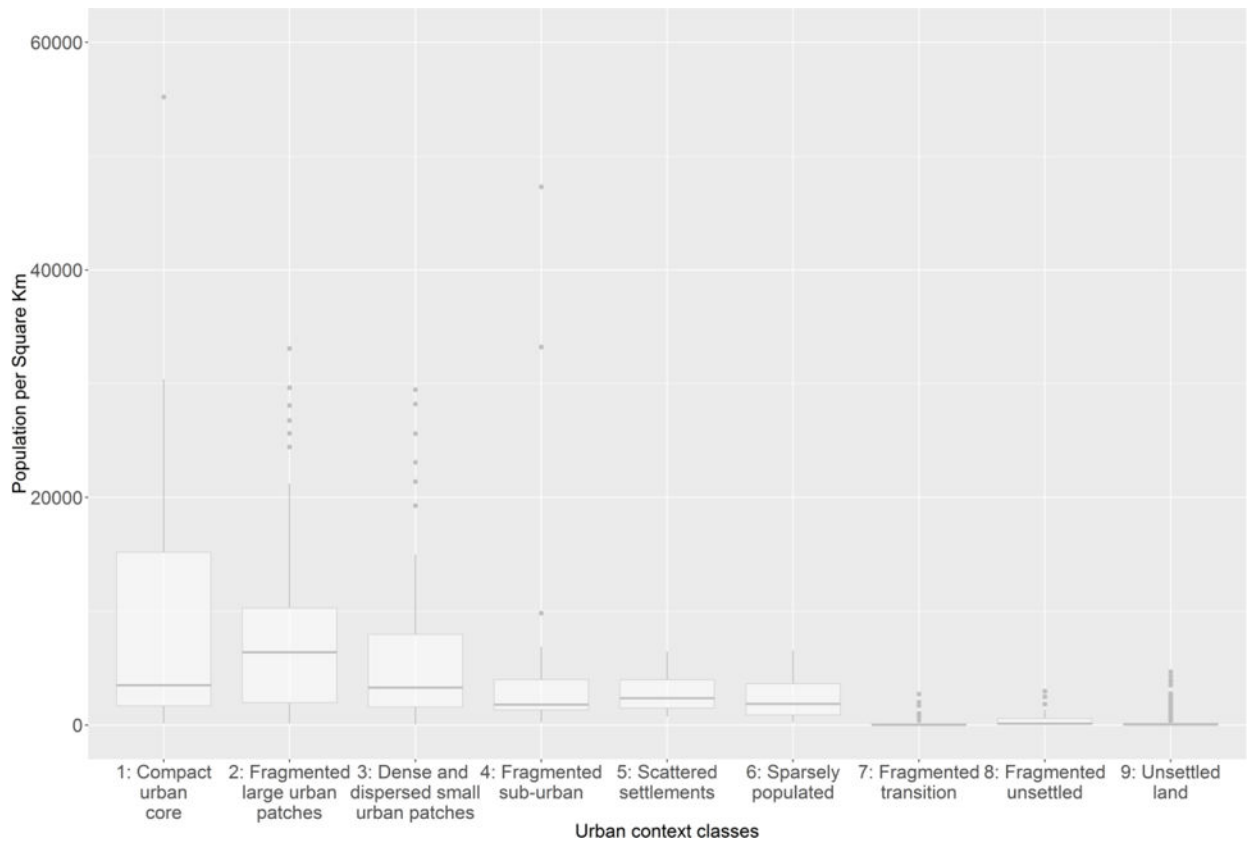
Figure 13.
Population density throughout the urban context classification. Population density is highest on the most urban end the scheme and decreases as classes transition into the most rural unsettled land.

Table 1

Urban context rules for classification of reference data in Google Earth

Class	Urban context class name	Rules
1	Compact urban core	More than 50% built, dense small buildings no vegetation
2	Fragmented large urban patches	More than 50% built, fragmented large buildings, little vegetation
3	Dense and dispersed urban patches	More than 50% built, fragmented small buildings, fragmented vegetation
4	Fragmented suburban	More than 25% built, fragmented buildings, significant vegetation
5	Scattered settlements	Less than 25% built, compact built and vegetation
6	Sparsely populated	Less than 25% built, fragmented built and vegetation
7	Fragmented transition	Less than 10% built, fragmented built
8	Fragmented unsettled	Less than 10% built, very little built
9	Unsettled land	No built, mostly vegetation

Table 2

Fuzzy accuracy linguistic score

Score	Assessment of prediction
1	Absolutely wrong
2	Understandable but wrong
3	Reasonable answer
4	Good answer
5	Absolutely right

Table 3

SMA based land cover classification confusion matrix

		Reference points				
		Built	Vegetation	Other	n reference points	user accuracy
classified as	Built	44	0	10	54	81
	Vegetation	0	473	60	533	89
	Other	8	9	396	413	96
n reference points		52	482	466	1000	
producer accuracy		85	98	85		
Overall agreement		91				

Table 4

Radar-based Built/Non-built classification confusion matrix

		Reference points			
		Built	Non-built	n reference points	user accuracy
Classified as	Built	48	24	72	67
	Non-built	3	825	828	100
n reference points		51	849	900	
producer accuracy		94	97		
Overall agreement		97			

Author Manuscript

Author Manuscript

Author Manuscript

Author Manuscript

Table 5

Urban context classification confusion matrix

		Reference cells									n reference cells	user accuracy
		1	2	3	4	5	6	7	8	9		
classified as	1	23	2	3	0	1	1	0	0	0	30	77
	2	7	20	5	0	0	0	0	0	0	32	63
	3	0	10	33	11	0	0	0	0	0	54	61
	4	0	0	6	33	0	1	0	0	0	40	83
	5	0	0	0	0	28	2	0	0	0	30	93
	6	0	0	0	0	2	27	3	2	0	34	79
	7	0	0	0	0	0	0	27	5	1	33	82
	8	0	0	0	0	0	0	0	17	7	24	71
	9	0	0	0	0	0	0	0	11	56	67	84
n class cells		30	32	47	44	31	31	30	35	64	344	
producer accuracy		77	63	70	75	90	87	90	49	88		
Overall agreement		77										

1: compact urban

2: Fragmented large urban patches

3: Fragmented dense and dispersed urban patches

4: Fragmented sub–urban

5: Scattered settlements

6: Sparsely populated

7: Fragmented transition

8: Fragmented unsettled

9: Unsettled

Table 6

Fuzzy accuracy

Class	Reference cells	Right class	% Right	Exact class	% Exact
1: compact urban	30	19	63	11	37
2: Fragmented large urban patches	33	23	70	16	48
3: Fragmented dense and dispersed urban patches	37	32	86	18	49
4: Fragmented sub-urban	32	31	97	22	69
5: Scattered settlements	31	30	97	23	74
6: Sparsely populated	32	30	94	18	56
7: Fragmented transition	47	37	79	18	38
8: Fragmented unsettled	37	37	100	30	81
9: Unsettled	98	88	90	74	76
	377	327	87	230	61